AIMS Materials Science, 9(3): 512–521.
DOI: 10.3934/matersci.2022030
Received: 05 March 2022
Revised: 23 May 2022
Accepted: 31 May 2022
Published: 27 June 2022

http://www.aimspress.com/journal/Materials

Research article

Propagation of corrosion induced fatigue crack in aluminum alloy

Pawan Kumar[1,*] and BB Verma[2]

[1] University of Johannesburg, Faculty of Engineering and the Built Environment, Department of Engineering Metallurgy, John Orr Building, DFC, 25 Louisa St, Doornfontein, Johannesburg, 2028, South Africa

[2] Department of Metallurgical and Materials Engineering, National Institute of Technology Rourkela 76908, India

* **Correspondence:** Email: pkumar@uj.ac.za; Tel: +27631588123.

Abstract: Aluminium is considered a green metal due to its environmental responsive characteristics. The 7475-T7351 aluminum alloy is extensively used in automotive and aerospace applications due to its light weight and high strength. In the present work, the effects of the corrosive environment on the high cycle fatigue (HCF) behaviors of the 7475-T7351 aluminum alloy was investigated. The aqueous solution of sodium chloride was used for solution treatment. The HCF test was performed on pre-cracked specimens using a servo-hydraulic universal testing machine, Instron 8800. The fractured specimens were characterized using a scanning electron microscope. It was observed that the crack propagation occurred through anodic dissolution at high stress and a significant crack tip blunting and crack extension occurred. However, no appreciable change in crack growth was noticed over the lower frequency range of 0.1 to 0.9 Hz. The slower growth rate envisages oxide debris formation between the cracked faces. When the alloy was treated under corrosive environments, the HCF tests depicted that the fatigue life reduces up to two orders of magnitude. The corrosion pits induced the crack initiation in stage-I at lower alternating stress; however, the fatigue crack growth rate (FCGR) was increased in the corrosive environment. The transition from stage-I to stage-II occurred at a lower stress intensity range (ΔK) level; it was due to the combined effects of corrosion, hydrogen embrittlement, active path dissolution, and stress concentration. The corrosion fatigue test at low frequency also depicted a slower FCGR as compared to its moderate frequency counterpart and showed an irregular crack growth behavior.

Keywords: aluminium alloy; solution treatment; high cycle fatigue; microstructure

Abbreviations: FCGR: Fatigue crack growth rate; FCG: Fatigue crack growth; HCF: High cycle fatigue; SIF: Stress intensity factor; aq. NaCl: aqueous solution of NaCl

1. Introduction

Aluminium is termed a green metal since it is an environmentally responsive metal. The recycling of it saves 95% of the energy, obligatory to produce aluminium from raw materials. It has wide applications in automotive and aerospace applications [1]. The body of the lightweight aircraft and its components are commonly made of a 7475-T7351 aluminum alloy. However, the engineering components made from such materials are subjected to the corrosive environment during service; which in turn envisages corrosion induced fatigue damage. The corrosion fatigue damages the materials due to cyclic stresses in aggressive environments [1]. The initial morphology such as precipitates, grain size, initial dislocation densities and substructures influences the mechanical properties and corrosion performance to a great extent. Rachele et al. reported the influence of deformation temperature which leads to the coalescence of precipitates and decreases the dislocation density; which results in a decrease in the mechanical and corrosion performance of such material [2]. Experimental studies have also shown that the surface pits in metals can act as the starting point to corrosion induced fatigue crack growth [3–5]. The aluminum alloys reduced their fatigue life by a factor of two to an order of magnitude due to the presence of such pits [6]. The fatigue crack growth rate (FCGR) also accelerated in the detrimental environment. It is also known that the adsorbed hydrogen (rather than the dissolved) is responsible for accelerated crack growth in a hydrogen bearing environment [7–9]. The aluminum alloys are usually exposed to an aqueous saline environment during service. Hence, the corrosion fatigue studies of such alloys are of practical significance. The prolonged spraying of salt water or fogging salt during service envisages the electrochemical reactions to occur in the material; and as a result, several pits form near the constituent particles [10]. These pits are the potential sites for crack initiation under fatigue loading [6]. The primary mechanism which diminishes the service life of such alloys in the saline atmosphere is the initiation of premature crack due to the formation of surface pits. It is also reported that the FCGR is enhanced in an aggressive environment which diminishes the fatigue performance of aluminum alloy [11]. The fatigue crack growth performance of 7475 aluminum alloy has been reported in an earlier work by the same author; however, its corrosion-fatigue characteristics have not been reported [12]. The fatigue behaviour of such materials was also studied in an aggressive environment but in a more conservative manner which only describes the microstructure characteristics at the lower stress intensity factor (SIF); it did not address the effect of higher stress intensity and alternating stress; also, the anodic dissolution was not considered [13]. Therefore, it feels that a more descriptive/elaborative approach is required to study the corrosion fatigue of such alloy considering a wide range of SIFs, stress intensity, alternating stress and also considering the influence of anodic dissolution on the corrosion fatigue. In the present investigation, the HCF behaviour of pre-cracked 7475-T7351 aluminum alloy subjected to a corrosive environment (using an aqueous solution of sodium chloride solution) at high stress and a frequency in the range of 0.1 to 0.9 Hz was studied using Instron 8800 servo hydraulic testing apparatus. The FCGR

vs stress intensity range (ΔK) curve was examined at various frequencies and the subsequent mechanism of fatigue crack growth (FCG) was studied. The influence of corrosion pits and anodic dissolution were also considered to examine the HCF behaviour for stage-I and stage-II at lower and higher stress intensity ranges, and fractographical studies were made to study the mechanism of crack growth.

2. Materials and methods

In the present work, 7475 aluminum alloy was used. The thickness of the material was 12.5 mm and the composition (in wt.%) material was 5.73Zn–2.14Mg–1.15Cu–0.05Fe and balance–Al. The as-received alloy was in T7351 condition. In T7351, the alloy is solution treated at 470 ℃ followed by water quenching and 1.5% to 3% stretching and further ageing for 25 h at 121 ℃ and for 24 to 30 h at 163 ℃. The as-received alloy showed a yield strength of 495 MPa and elongation of 14%. The specimens for the high-cycle fatigue test were taken from the as-received sample. The details of specimen dimensions are shown in Figure 1a. HCF tests in load-controlled mode at a load of 100 kN were carried out on servo-hydraulic equipment. Cycles with sinusoidal loads and stress ratio (R) of −1, that is complete push-pull were applied for all the tests. The tests for fatigue in the air were directed at a 3 Hz frequency. The tests for an open potential environment were performed in a plastic container having 3.5% NaCl (aq. sol.) having a pH of 8.2 at ambient temperature. All the environmental tests were conducted at a 1 Hz frequency. The crack growth studies were conducted on CT samples. The specimens having a 12.5 mm thickness and a 50 mm width were cut in the T–L orientation. Figure 1b depicts the details of CT specimen dimensions. The test specimens were polished and degreased. A pre-crack of length 17 mm (a/w~0.34) was made on the specimen. FCGR investigation was performed on pre-cracked specimens. The loading condition was tension-tension with sinusoidal loading and a stress ratio (R) of 0.2. A constant range of load was applied for experiments. 1 Hz of frequency was applied to air test conditions. The FCG tests were conducted in the above-mentioned aqueous solution at frequencies of 0.02, 0.1, 0.17, 0.45, and 0.90 Hz. The extents of extension in crack were recorded with the help of the direct current potential drop technique. The fractured specimens of high-cycle fatigue tests were thoroughly cleaned with the help of cellulose film and also in an ultrasonic bath with acetone and subsequently examined under the field emission scanning electron microscope operated at a voltage of 20 kV with a working distance of 10 mm.

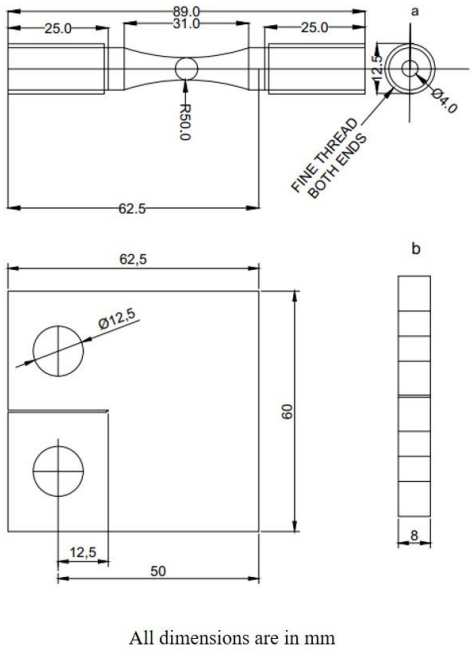

Figure 1. Dimensional details of (a) HCF test specimen and (b) CT-specimen.

3. Results and discussion

3.1. Effect of the aqueous solution of NaCl (aq. NaCl) on S-N curve

The fatigue life of the specimen was characterized for alternating stress. The results from uniaxial compression-tension cyclic loading in the air and aq. NaCl is shown in Figure 2. It was observed that in the case of loading in the air, at the alternating stress of 250 MPa, the number of cycles to failure was 1.05×10^5. The fatigue life cycle increased to 2.07×10^6 upon decreasing the alternating stress level to 187 MPa. Expectedly, the behaviors of fatigue in air and NaCl environment were significant. The S–N curve dropped downward on changing the environment from air to saline water. For having a fatigue life cycle of 1×10^6 numbers of cycles, the required stress level in the case of air is 240 MPa whereas in the case of saline water it is 170 MPa. It is suggested that this decrease in stress was attributed to the formation of pits in saline water solution, and act as sites for stress concentration. A similar influence of such pits was also reported by other researchers [14]. The microstructure obtained from the pre-cracked specimens tested in aq. NaCl for different alternating stresses is shown in Figure 3. It was observed to be intergranular corrosion in the early stage as shown in Figure 3a. The severe stress concentrating pits, generated on the surface was identified as crack nucleating sites. The crack nucleation has been found to occur at several points by localized pits formation. It is also reported that these pits transform into cracks when they attend critical sizes for the threshold SIF or the FCGR exceeds the pit growth rate [15]. The folded depressions along with the particles on the surface envisage localized dissolution of the matrix because of local galvanic cell creation as shown in Figure 3a. It is further suggested that open space around the particle at the surface and tunnels are the indications of diffusion of electrolyte into the material and substantial corrosion beneath the surface as shown in Figure 3b. A single pit has also given rise to a number (2–3) of separate cracks as evident

from Figure 3a,b. It specifies that the corrosion pits were accountable for the primary crack initiation and stage-I crack extension. It was also observed that the crack nucleated from the pit was not always started from the tip of the pits but from the sidewalls of pits as well which is evident in Figure 3a. Therefore, the corrosive environment has contributed to the subsequent flat grain facets and featureless extension of the crack, characterizing the stage-I crack extension. It indicates the transition of corrosion pits to stage-I fatigue in the early stage. There also exists a competition between pitting corrosion and FCG which is a transition from corrosion pitting to crack development. When the altering stress (S = 200 MPa) was higher, corrosion pits and tunnels were not observed as shown in Figure 3c. Since cyclic stress intensity range (ΔK) for a pit must exceed the threshold value of stress intensity range (ΔK_{th}) for its extension as a fatigue crack, the reduction in corrosion pit size with increasing applied stress amplitude; therefore it indicates the early achievement of the required ΔK_{th} for the occurrence of pitting to fatigue crack transition. It is suggested that the FCG occurred through anodic slip dissolution and higher stress provided the driving force. The beach mark which is an indication of FCG is shown in Figure 3c.

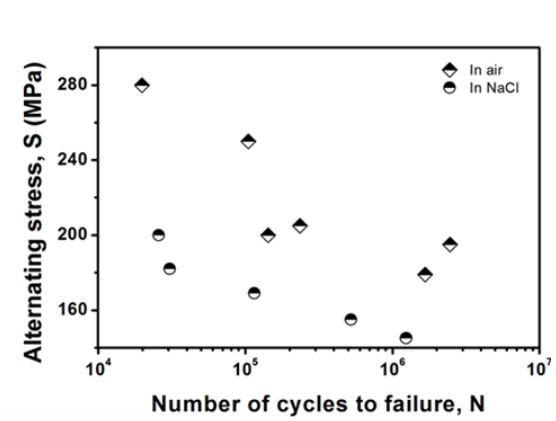

Figure 2. Variation in alternating stress and number of cycles to failure in air and saline environment.

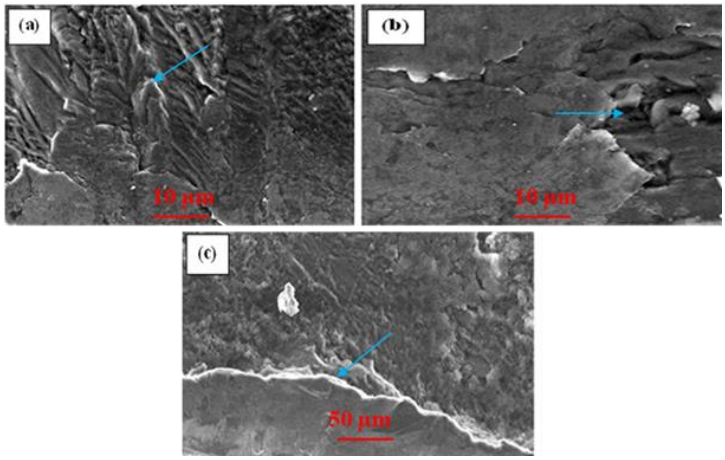

Figure 3. Microstructure of life estimation specimens tested in aq. NaCl at (a) alternating stresses of 145 MPa showing corrosion pits (b) another fracture surface of alternating stress 145 MPa showing corrosion beneath the surface (c) alternating stresses of 200 MPa showing beach mark.

3.2. Effect of the aq. NaCl on crack growth behavior

During crack growth in corrosion fatigue, the bare surface of metal comes in contact with a corrosive environment. The chemical reaction occurring on exposure of aluminum alloy to the aq. NaCl is by Eq 1:

$$Al \rightarrow Al^{3+} + 3e \quad (1)$$

It is known that the above chemical reaction and anodic dissolution, result in the consumption of the metal at the crack tip causing crack extension other than the mechanical fatigue; the simultaneous cathodic reaction produces atomic hydrogen and subsequently diffuses into the alloy [16,17]. The FCGR of the alloy at a stress ratio (R) of 0.1 in air and aq. NaCl as a function of ΔK is shown in Figure 4. The figure demonstrates that the FCGR was increased due to the introduction of saline water during the test. It is just like to achieve a suitable growth rate of 5.0×10^{-8} m/cycle, the required ΔK in the air is ≈ 9.2 MPa√m; whereas the same diminished to ≈ 8.0 MPa√m when the test was conducted in saline water. At ΔK of 10.0 MPa√m, the replacement of air with salt water showed about a fourfold increment in FCGR.

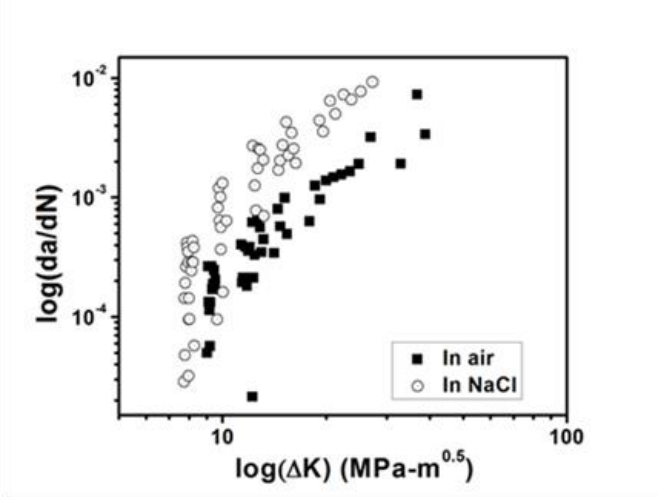

Figure 4. Variation of FCGR with logΔK in air and aq. NaCl.

The FCGR frequency has been known to be a critical variable in the corrosion fatigue of high strength Al-alloys. The results of variations in FCGR with ΔK under varying frequencies are shown in Figure 5. The air test data was also incorporated to visualize an overall effect. The results indicated the enhancement of FCGR due to the presence of a corrosive environment in all cases. There was no appreciable change in FCGR with frequency (in the range of 0.1 to 0.9 Hz). However, 0.02 Hz test data did show a slower growth rate compared to all other environmental test results. It is also important to note that at a low ΔK level, there was a progressive increase in FCGR in all the environmental tests except the test conducted at a frequency of 0.02 Hz. The environmental test conducted at 0.02 Hz exhibited a progressive decrease in growth rate till $\Delta K \approx 9.00$ MPa√m, a feature common in short fatigue crack, followed by an increase in growth rate characterizing long crfack growth behaviour.

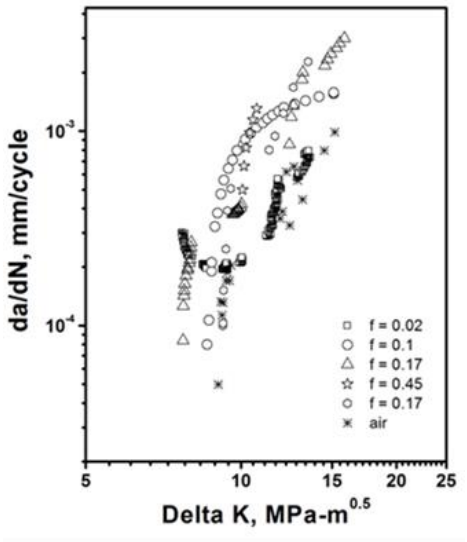

Figure 5. Variation in FCGR with ΔK under varying frequencies.

The *a–N* curve (Figure 6) generated by the FCG test conducted at a frequency of 0.02 Hz did not show a regular increase in FCGR, especially in the low ΔK region. It indicates the presence of two fundamental interactions of mechanical and chemical forces as they cause transient breaking and reformation of passive films. It also supports the hypothesis that the corrosion products at the crack tips under sustained loading conditions act to protect the material surfaces from the environmental attack, but are ruptured by cyclic loading, thereby permitting the corrodent to re-attack the crack tip region; a similar observation was also reported by Gingell et al [14]. The *a–N* plot (Figure 6) at 0.02 Hz frequency followed an unusual growth pattern, low height peaks and shallow valleys for a few thousand cycles followed by a high peak, indicating a burst in crack extension at regular intervals. This was a characteristic of hydrogen embitterment induced crack growth.

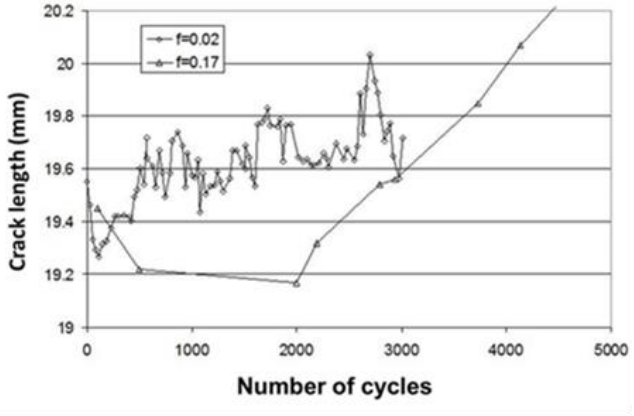

Figure 6. Variations in crack length and number of cycles during environmental test at 0.17 and 0.02 Hz.

3.3. Microstructure

The microstructure of fracture surfaces subjected to FCG test (in air and aq. NaCl) are presented in Figures 7 and 8, respectively. The SEM microstructure of the specimen tested in air at a $\Delta K \approx 9.00$ MPa√m is presented in Figure 7a. The microstructure shows the grain facets and striations transverse to the crack growth direction (coarse striations). The striation spacing was around 0.51 μm, which is much higher than the macroscopic FCGR for the same ΔK level which is 0.15 μm/ cycle. It is also suggested that these microstructural characteristics were associated with crack propagation which did not occur cycle by cycle but rather occurred intermittently. Figure 7b illustrates the microstructure of the same specimen at a higher $\Delta K \approx 13.00$ MPa√m. It indicates the ductile striations perpendicular to the crack growth direction. The striation spacing in this region is almost equal to the macroscopic FCGR which indicated the cycle-by-cycle extension of the crack. Microstructure in Figure 7a,b shows the difference in the features of the striations developed at the two investigated ΔK levels. At the low ΔK test, striations appear to be brittle in nature without a sign of appreciable blunting of the crack tip during its growth. On the other hand, striations produced at $\Delta K \approx 13.00$ MPa√m revealed significant crack blunting during its growth.

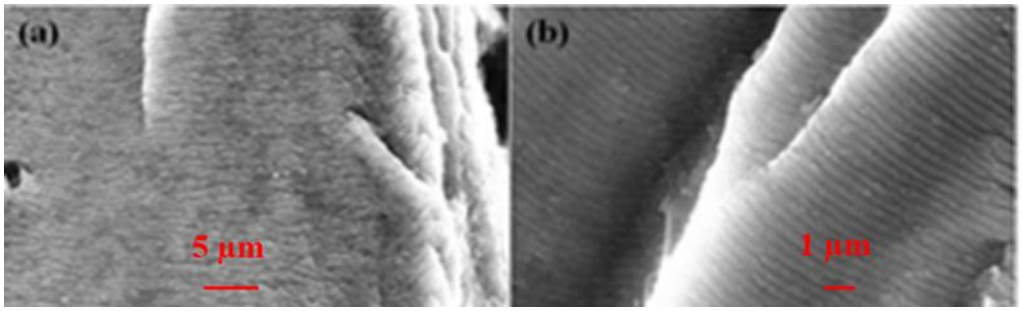

Figure 7. Fractography of broken CT-specimens tested in air at (a) $\Delta K \approx 9.0$ MPa√m and (b) $\Delta K \approx 13.0$ MPa√m.

The FCGR test of the specimens at a frequency of 0.17 Hz resulted in a modification in the characteristics of the fracture surface as shown in Figure 8a,b. At a $\Delta K \approx 8.7$ MPa√m, the flat facets were replaced by surface corroded grains, which was the indication of intergranular corrosion. Brittle striations were found on the surface of the grains, although their appearances are not clearly defined as shown in Figure 8a. The macroscopic FCGR at a $\Delta K \approx 8.7$ MPa√m was around 0.70 μm. The microstructure of the same specimen at a higher $\Delta K \approx 10.5$ MPa√m exhibited the grain facets extensively enclosed with brittle striations and striation spacing equivalent to the macroscopic growth as shown in Figure 8b. Therefore, the transition from stage I to stage II FCG was suggested. The microstructure of the specimen tested in NaCl solution at 0.02 Hz is shown in Figure 8c,d. Figure 8c represents the microstructure at a $\Delta K \approx 8.7$ MPa√m (stage-I region). It showed the grains which were completely covered with corrosion indicated a transgranular fracture. It is suggested that the FCG test at a frequency of 0.17 Hz did show a similar feature indicating the dominance of corrosion pit formation at a low level of SIF. Brittle striations were covered with dip corrosion pits at $\Delta K \approx 10.5$ MPa√m (stage-II) and shown in Figure 8d.

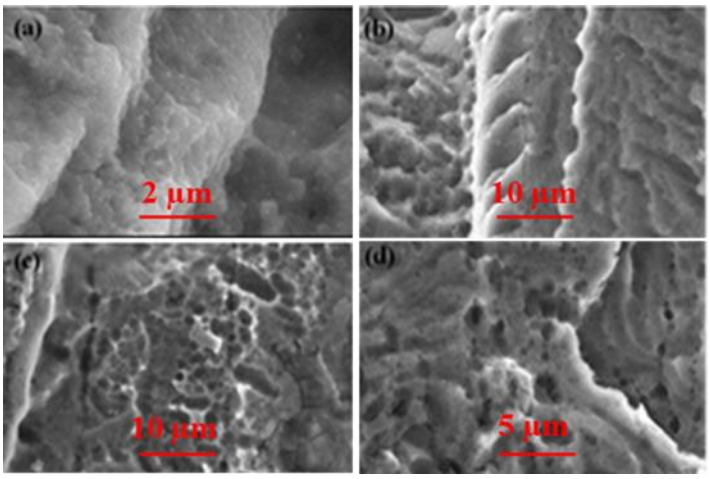

Figure 8. Fractography of broken CT-specimens tested in NaCl at (a) $\Delta K \approx 8.53$ MPa√m (f = 0.17), (b) $\Delta K \approx 10.5$ MPa√m (f = 0.17), (c) $\Delta K \approx 8.53$ MPa√m (f = 0.02) and (d) $\Delta K \approx 10.5$ MPa√m (f = 0.02).

4. Conclusion

The conducted experiments and their pertinent analyses lead to the following conclusions:

1. The HCF tests were conducted in air and corrosive environments. The results indicated that fatigue life reduced up to two orders of magnitude under the influence of corrosive environments.
2. Corrosion pits were responsible for early crack initiation and stage-I crack extension at low alternating stress in aq. NaCl. However, at high stress levels, crack initiation and propagation occurred through anodic dissolution. No appreciable change in crack growth was noticed over the frequency range of 0.1 to 0.9 Hz. The low frequency environmental test exhibited a slower growth rate than the moderate frequency test, due to a large amount of oxide debris formation between the cracked faces and its inability to get dislodged. It shows a short fatigue crack behavior.
3. In air test, there was significant crack tip blunting controlled crack extension at a high ΔK level. The environmental test exhibited corrosion pit dominated crack growth in stage-I. While in stage-II, the brittle striation induced extension was observed.

Conflicts of Interest

The authors declare no conflict of interest.

References

1. Bayoumi MR (1993) Fatigue behaviour of a commercial aluminium alloy in sea water at different temperatures. *Eng Fract Mech* 45: 297–307. https://doi.org/10.1016/0013-7944(93)90015-K
2. Bertolini R, Simonetto E, Pezzato L, et al. (2021) Mechanical and corrosion resistance properties of AA7075-T6 sub-zero formed sheets. *Int J Adv Manuf Technol* 115: 2801–2824. https://doi.org/10.1007/s00170-021-07333-7

3. Hoeppner DW, Arriscorreta CA (2012) Exfoliation corrosion and pitting corrosion and their role in fatigue predictive modeling: State-of-the-art review. *Int J Aerosp Eng* 2012: 1–29. https://doi.org/10.1155/2012/191879
4. Sharma MM, Tomedi JD, Parks JM (2015) A microscopic study on the corrosion fatigue of ultra-fine grained and conventional Al–Mg alloy. *Corros Sci* 93: 180–190. https://doi.org/10.1016/j.corsci.2015.01.020
5. El May M, Palin-Luc T, Saintier N, et al. (2013) Effect of corrosion on the high cycle fatigue strength of martensitic stainless steel X12CrNiMoV12-3. *Int J Fatigue* 47: 330–339. https://doi.org/10.1016/j.ijfatigue.2012.09.018
6. Wang QY, Kawagoishi N, Chen Q (2003) Effect of pitting corrosion on very high cycle fatigue behavior. *Scr Mater* 49: 711–716. https://doi.org/10.1016/S1359-6462(03)00365-8
7. Ricker RE, Duquette DJ (1988) The role of hydrogen in corrosion fatigue of high purity Al–Zn–Mg exposed to water vapor. *Metall Trans A* 19: 1775–1783. https://doi.org/10.1007/BF02645146
8. Pérez-Mora R, Palin-Luc T, Bathias C, et al. (2015) Very high cycle fatigue of a high strength steel under sea water corrosion: A strong corrosion and mechanical damage coupling. *Int J Fatigue* 74: 156–165. https://doi.org/10.1016/j.ijfatigue.2015.01.004
9. Bradshaw FJ, Wheeler C (1969) The influence of gaseous environment and fatigue frequency on the growth of fatigue cracks in some aluminum alloys. *Int J Fract Mech* 5: 255–268. https://doi.org/10.1007/BF00190956
10. DuQuesnay DL, Underhill PR, Britt HJ (2003) Fatigue crack growth from corrosion damage in 7075-T6511 aluminium alloy under aircraft loading. *Int J Fatigue* 25: 371–377. https://doi.org/10.1016/S0142-1123(02)00168-8
11. Hamano R (1996) On the transition of fatigue crack growth from stage i to stage II in a corrosive environment. *Metall Mater Trans A* 27, 471–476. https://doi.org/10.1007/BF02648426
12. Verma BB, Atkinson JD, Kumar M (2001) Study of fatigue behaviour of 7475 aluminium alloy. *Bull Mater Sci* 24: 231–236. https://doi.org/10.1007/BF02710107
13. Verma BB, Mallik M, Atkinson JD, et al. (2012) Fatigue crack initiation and growth behavior of 7475 Aluminium alloy in air and aggressive environment. *Adv Mater Res* 428: 133–136. https://doi.org/10.4028/www.scientific.net/AMR.428.133
14. Gingell ADB, King JE (1997) The effect of frequency and microstructure on corrosion fatigue crack propagation in high strength aluminium alloys. *Acta Mater* 45, 3855–3870. https://doi.org/10.1016/S1359-6454(97)00033-5
15. Jahn MT, Luo J (1988) Tensile and fatigue properties of a thermomechanically treated 7475 aluminium alloy. *J Mater Sci* 23: 4115–4120.
16. Wang R (2008) A fracture model of corrosion fatigue crack propagation of aluminum alloys based on the material elements fracture ahead of a crack tip. *Int J Fatigue* 30: 1376–1386. https://doi.org/10.1016/j.ijfatigue.2007.10.007
17. Dieter GE, Bacon D (1976) *Mechanical Metallurgy*, New York: McGraw-Hill.

AIMS Press